

# Optimization of CMT Welding Parameters of Stellite-6 on AISI316L Alloy Using TOPSIS Method

Thinesh Babu Thiagarajan<sup>1\*</sup>, Raguraman D<sup>2</sup>, Sengottuvel Ponnusamy<sup>2</sup>

<sup>1</sup>Research Scholar –Bharath Institute of Higher Education and Research, Chennai, 600073, INDIA

<sup>2</sup>Research Supervisor –Bharath Institute of Higher Education and Research, Chennai, 600073, INDIA

\*Corresponding Author

DOI: <https://doi.org/10.30880/ijie.2023.15.01.014>

Received 17 August 2021; Accepted 28 October 2021; Available online 28 February 2023

**Abstract:** This article discusses the welding parameters optimization to find the quality of stellite-6 cladding on AISI304L austenite alloy using a new optimization method called Technique for Order of Preference by Similarity to Ideal Solution (TOPSIS). The experiments (31 nos.) were carried out with the cold metal arc transfer welding method (CMT) based on the central composite design (CCD). The cladding material is the stellite-6 alloy which is appreciated for its corrosion and wear resistance. Four factors (welding current, voltage, welding speed and torch angle) and five levels were considered for the experiment and the optimization. It is necessary to find the optimized parameters for the industrial applications as a huge number of experiments are not recommended. The optimization results showed that the 2nd experiment had the 1st rank with high relative closeness and the 19th experiment was in the last rank. Higher current and low welding speed yielded good results and a low corrosion rate of 0.004582 mm/yr. Furthermore, the Micro-structural, Corrosion study and the SEM-EDS of the specimen produced by the 2nd experiment are discussed here. Cr and Co elements were most abundant, according to an EDS study, in the cladding region.

**Keywords:** Cladding, CCD, CMT, Stellite-6, TOPSIS, optimization, SEM, EDAX, corrosion resistance

## 1. Introduction

The new welding techniques are suggested to improve the performance of weld quality and save energy. CMT is one of the advanced welding techniques of the metal inert gas welding (MIG) group. CMT can be performed for the cladding process. There is numerous competitive welding process for the CMT cladding like TIG, MIG, Laser, plasma transferred arc welding, plasma hard facing, shielded metal arc welding and high-velocity oxy-fuel coating method called HVOF used for the cladding process. Laser cladding was one of the popular processes among the others and the research on it is plenty [1]. HVOF shows better performance particularly on abrasive wear, while the TIG process with hot wire process showed the resistance in corrosion of material [2]. Evangeline.A et al [3] used TIG process for cladding the Ni based alloy over 316L alloy. The results showed that TIG was efficient and formed the dimple fracture in the tensile samples. CMT process only required low heat input for its process and has low dilution during the process. As this low heat input increases the joint efficiency, CMT is famous and widely used in industries. Most of the literature recommended the stellite alloy coating due to its appreciable properties and it is a cobalt-based alloy. Stellite has an FCC structure. According to Mohammed, S et al. [4], laser cladding improved the corrosion, wear and mechanical properties of fiber steel cladding and showed that the process parameters was deciding the cladding surface geometry. Using the TIG technique, G.R. Mirshekari et al. [5] investigated the cladding of stellite-6 on the surface of SS420 alloy. The research showed that the stellite-6 cladding surface had the presence of carbide into the cobalt-rich phase. The dilution of the stellite-6 can be restricted by other stainless steel metal or the stellite interlayers. In the inconel cladding research, the CMT process produced a large reinforcement compared to the plasma arc welding (PAW); whereas PAW developed a

\*Corresponding author: [thineshabu@outlook.com](mailto:thineshabu@outlook.com)

2023 UTHM Publisher. All rights reserved.

[penerbit.uthm.edu.my/ojs/index.php/ijie](http://penerbit.uthm.edu.my/ojs/index.php/ijie)

good surface, and a maximum dilution rate [6]. The CMT process is recommended for wire-arc deposition and can be used for inconel cladding with AC current [7]. Zinke, M et al. [8] informed through their research that CMT process produced no weld defects, no porosity and low dilution. Ganesh et al. [9] studied the fracture behaviour of stellite-21 category alloy on the SS316L alloy and recommended the laser cladding process as it increased fatigue strength. G.P.Rajeev [10] used the CMT process for hard facing on H13 die steel by stellite 21. The authors said that thick cladding was possible by the CMT process and showed no cracking on the heat-treated substrate. Anish Nair et al. [11] discussed the cladding of stellite-6 co-based alloy over the metal EN8 steel using laser cladding as it is a popular method. The corrosion index was optimized by the fuzzy model and the Taguchi method. The fuzzy values were converted into the crisp output values when the optimization took place. Further, the crisp output was used for the Taguchi analysis to identify the optimum values in the cladding process. G.P Rajeev et al. [12] suggested through their research using CMT process that CMT is an energy efficient cladding technique and a good method which can produce thick coating with no porosity and low dilution. Using response surface methodology, F.Madadi et al. [13] optimized the stellite cladding created by the pulsed TIG method (RSM). Mathematical modelling was used for optimizing the cooling rate and heat input. The author developed a mathematical modelling second order regression for studying the correlations. The RSM results were very close to the experimental results. Thus the optimization helps improve the welding performance. TOPSIS is a well-established multi-criteria decision-making technique [14] that helps find the ideal solutions and can be used for financial business [15]. Generally, algorithms are used for analysing the results to get the optimized solution. TOPSIS was developed to rank the process and to evaluate the algorithms through mean and standard deviations [16]. The TOPSIS method was used by Robbi Rahim et al. [17] to choose the best employees in the sector. Xing Zhongyou [18] agreed through his research that that TOPSIS is having high applicability to comprehensively evaluate the players' ability and gave good results. Though TOPSIS is an effective method, some shortcomings were found in solving multi-criteria decision-making problems (MCDM) [19]. So, some of the alternatives like D-TOPSIS, A-TOPSIS, m-Polar TOPSIS etc were newly proposed in the literature. Dariusz Kacprzak [20] framed a new kind of TOPSIS approach with fuzzy numbers for the ranking and successfully solved MCDM problems. Also, the RSM-TOPSIS-IN hybrid method can be used for MCDM problems [21]. Marzban, J.et al. [22] proved the use of TOPSIS optimization in the laser cladding of AISI 1040 to find the optimal surface parameters. The results showed the best performance of laser cladding on the metal comparing to other competitive processes. Focus has been placed on the magnesium AZ91D alloy with machined Polycrystalline diamond (PCD) cutting inserts by Ramesh et al. [23]. They have applied two optimization techniques like TOPSIS, GRA and RSA for optimize the machined components of surface roughness and tool flank wear. Linear and quadratic model equations were used for predict the expected outcomes of the experiments. Their findings showed that the feed rate and cutting speed were the two main factors impacting surface roughness and flank wear, respectively. And it was found that the predicted values and the measured values are very close to each other. Regarding the corrosion behaviour of the EBW joints, Ramesh et al. [24] have concentrated on the electron beam welding parameters of nickel-based super alloy and stainless steel joints. They have applied Taguchi method in order to optimize the number of experiments to be performed in EBW process. To evaluate the corrosion behaviour of welded materials, the weld joints were constructed in accordance with the parametric design, and potentiodynamic polarization was applied to the weldments in a 5% NaCl environment.

The objective of this work is to optimise the CMT stellite-6 cladding process parameters using the new method called TOPSIS and categorize the experiments by the ranking. Likewise, the specimens of the tests with the first rank, middle rank, and last rank are characterised to analyse the cladding performance in accordance with the optimization results. The steps of the TOPSIS method are also explained here in detail. The application of TOPSIS in the welding and cladding process is lacking in the literature and this paper is satisfying it.

## 2. Material and Method

The cobalt-based alloy stellite-6 (chemical composition in weight: 1.15% C, 28% Cr, 4% W, 1.3% Fe, 1.1% Si, 0.06% Mn and cobalt is remaining) was the cladding metal in the form of filler wire and the SS316L alloy (chemical composition in weight: 0.03% C, 2% Mn, 0.75% Si, 16-18% Cr, 10-14 % Ni, 2-3% Mo, 0.045% P, 0.03% S, 0.1% N and Fe is remaining). Stellite-6 is excellent in erosion, corrosion and wears properties [25, 26]. A low carbon SS316L stainless steel is having good weldability and suitable for cladding applications, where the alphabetical letter 'L' in suffix is meant for low carbon content [27]. The cladding of stellite-6 filler wire of size  $\phi 1.2$  diameter on the metal 316L sheet of size 420 mm length and 20 mm width was performed using the CMT method which is an advanced process of MIG/gas metal arc welding (GMAW). The welding materials were cleaned with acetone to remove the dirt. The experiments were followed as per the welding conditions given in Tables 1 and 2 outlined by CCD. The welding parameters were further optimized using the new optimization techniques called TOPSIS. One of the advanced and reliable approaches to MCDM problems is 'TOPSIS' and it was first introduced by Hwang and Yoon [21] to attain the optimum alternative based on the principle of compromise result. The desired result can be described as favouring the reaction that takes the shortest path to the ideal limit that is favourable and the longest path to the ideal limit that is unfavourable. Macrostructure and microstructure were taken using the microscope Dewinter optical tech. Geminis SEM 300 Carlzeiss equipment attached with EDS was used for taking the SEM images and for doing the EDS.

**Table 1 - Welding parameters and their levels**

Parameters	Notation	-2	-1	0	+1	+2
Welding Current (Amps)	I	120	140	160	180	200
Voltage (v)	V	15	17	19	21	23
Torch Angle(deg)	TA	50	60	70	80	90
Welding Speed(m/min)	TS	100	125	150	175	200

### 3. Results and Discussion

#### 3.1 TOPSIS Optimization

When there are several distinct parameters combinations available, it is crucial to choose the ideal one for welding. Model calculations are shown in the Appendix-A for first set of experimental result. A multi-criteria decision-making (MCDM) problem entails selecting the best set of parameters from all of the potential options. Generally, an MCDM problem is expressed comfortably in a matrix form as in equations 1 and 2.

$$D = \begin{matrix} & C_1 & C_2 & \dots & C_n \\ \begin{matrix} P_1 \\ P_2 \\ \vdots \\ P_m \end{matrix} & \begin{bmatrix} x_1(1) & x_1(2) & \dots & x_1(n) \\ x_2(1) & x_2(2) & \dots & x_2(n) \\ \vdots & \vdots & \ddots & \vdots \\ x_n(1) & x_n(2) & \dots & x_n(n) \end{bmatrix} \end{matrix} \tag{1}$$

$$W = [w_1 \ w_2 \ \dots \ w_m] \tag{2}$$

where  $P_1, P_2, \dots, P_m$  are the possible parameter combinations (trial runs) among which the best parameter combination should be selected;  $C_1, C_2, \dots, C_n$  are criteria by which the performance alternatives are determined;  $x_i(j)$  is the rating of the combination  $P_i$  with respect to  $C_j$ ; and  $w_j$  is the weight of criterion  $C_j$ .

The TOPSIS methodology is used to choose the best alternative in the subsequent steps.

Step 1: Since they are essential for describing the type of problem, it is first important to identify the dependent parameters and independent parameters. The most desirable dependent parameters are those that require maximising functions, while the least desirable dependent parameters are those that demand minimization functions.

In the current study, the output parameters for hardness and depth of penetration must be maximised and are therefore regarded as the most desirable features. The remaining output parameters must be minimised and are therefore regarded as the least desirable attributes. The output's quality and productivity can be raised by optimising the answers.

Step 2: The data relating to the output responses must be stated in terms of a matrix with I rows (m alternatives) and j columns, which is frequently referred to as a decision matrix (n - criteria).

$$[D_{31 \times 5}] = \begin{pmatrix} 2.744 & 31.618 & 351 & 0.000781 & 0.079 \\ \vdots & \vdots & \vdots & \vdots & \vdots \\ \vdots & \vdots & \vdots & \vdots & \vdots \\ 1.858 & 30.346 & 336 & 0.004062 & 0.054 \end{pmatrix} \tag{3}$$

The decision matrix  $[D_{31 \times 5}]$  of the present work is given in Eq. (1).

Step 3: The decision matrix from the prior stage is normalised, and the following equation [Eq. (2)] is used to calculate each element of the matrix.  $N_{ij}$  is used to represent the normalised matrix.

$$N_{ij} = \frac{x_{ij}}{\sqrt{\sum_{i=1}^m x_{ij}^2}} \quad j = 1, 2, \dots, n \tag{4}$$

**Table 2 - Experimental matrix based on CCD & normalized decision matrix**

Si.No.	I (Amps)	V (V)	TA (deg)	TS (m/min)	Depth of Penetration	Weld Area	Hardness of the clad	Corrosion rate	Interface Thickness
1.	140	17	60	125	0.214422	0.200635	0.18185	0.005042	0.162674
2.	180	17	60	125	0.126981	0.124405	0.180814	0.029579	0.102958
3.	140	21	60	125	0.171913	0.171331	0.183404	0.134595	0.205917
4.	180	21	60	125	0.225518	0.208199	0.184959	0.060584	0.146201
5.	140	17	80	125	0.177461	0.160931	0.185477	0.069138	0.189443
6.	180	17	80	125	0.226612	0.218288	0.166307	0.058286	0.205917
7.	140	21	80	125	0.164099	0.177042	0.167343	0.021884	0.205917
8.	180	21	80	125	0.212	0.184777	0.18185	0.013318	0.146201
9.	140	17	60	175	0.19223	0.166585	0.176151	0.019754	0.162674
10	180	17	60	175	0.247711	0.256279	0.169934	0.056046	0.117372
11	140	21	60	175	0.205045	0.349122	0.173561	0.043742	0.234745
12	180	21	60	175	0.158472	0.133422	0.182368	0.541739	0.105017
13	140	17	80	175	0.165193	0.144464	0.180296	0.00896	0.144142
14	180	17	80	175	0.133154	0.17951	0.177187	0.185141	0.175029
15	140	21	80	175	0.190433	0.178438	0.190658	0.029346	0.179147
16	180	21	80	175	0.201138	0.19335	0.183922	0.124073	0.22239
17	120	19	70	150	0.181134	0.147529	0.185477	0.417988	0.22239
18	200	19	70	150	0.180509	0.156159	0.196357	0.007462	0.105017
19	160	15	70	150	0.210437	0.181478	0.172006	0.55607	0.156497
20	160	23	70	150	0.189104	0.174574	0.173561	0.007966	0.140023
21	160	19	50	150	0.182462	0.161495	0.189103	0.181139	0.125609
22	160	19	90	150	0.146517	0.124729	0.180296	0.007469	0.210035
23	160	19	70	100	0.163786	0.133784	0.18185	0.005506	0.09884
24	160	19	70	200	0.150502	0.158818	0.185477	0.030308	0.144142
25	160	19	70	150	0.17457	0.172594	0.183922	0.027171	0.156497
26	160	19	70	150	0.151908	0.157098	0.164753	0.028281	0.393301
27	160	19	70	150	0.154487	0.153398	0.17097	0.012388	0.09884
28	160	19	70	150	0.155816	0.139831	0.177705	0.023375	0.175029
29	160	19	70	150	0.13714	0.155188	0.183404	0.313281	0.111195
30	160	19	70	150	0.155894	0.155118	0.178223	0.002756	0.280047
31	160	19	70	150	0.145188	0.192563	0.174079	0.026222	0.111195

The first and last elements normalised data are calculated using the following formula.

$$N_{1 \times 1} = \frac{2.744}{\sqrt{(2.744^2 + 1.625^2 + \dots + 1.858^2)}} = 0.214$$

$$\vdots$$

$$N_{31 \times 5} = \frac{0.054}{\sqrt{(0.079^2 + 0.05^2 + \dots + 0.054^2)}} \quad j = 0.111 \tag{5}$$

$$[N_{31 \times 5}] = \begin{pmatrix} 0.2144 & 0.2006 & 0.1818 & 0.0024 & 0.1626 \\ \vdots & \vdots & \vdots & \vdots & \vdots \\ 0.1451 & 0.1925 & 0.1740 & 0.0125 & 0.1111 \end{pmatrix} \tag{6}$$

The normalized decision matrix [N31×5] computed is shown in Eq. (6) and in table 2.

Step 4: The elements of the normalized decision matrix are then multiplied by their corresponding weights to create a weighted normalized decision matrix.

$$W_{ij} = N_{ij} \times W_j \tag{7}$$

Where Nij represents the normalized matrix and Wj represents the weight criteria. The weights (Wj) of each criterion are chosen with the aid of experts. The remaining characteristics are given a weight of 0.1, while the depth of penetration and hardness is given a weight of 0.35 because they are the most desirable. Using Eq., the components of the resulting weighted normalized matrix W31x5 are calculated (8).

$$\begin{aligned} W_{1 \times 1} &= 0.2144 \times 0.35 \\ W_{1 \times 2} &= 0.2006 \times 0.1 \\ W_{1 \times 3} &= 0.1818 \times 0.35 \\ W_{1 \times 4} &= 0.0024 \times 0.1 \end{aligned} \tag{8}$$

$$[D_{31 \times 5}] = \begin{pmatrix} W_{31 \times 5} = 0.1111 \times 0.1 \\ 0.0750 & 0.0200 & 0.0636 & 0.0002 & 0.0162 \\ \vdots & \vdots & \vdots & \vdots & \vdots \\ 0.0508 & 0.0192 & 0.0609 & 0.0012 & 0.0111 \end{pmatrix} \tag{9}$$

The final weighted normalized matrix [W31×5] is shown in Eq. (9).

Step 5: This step determines the positive ideal (A\*\*) and the negative ideal (A\*) solutions. These are calculated by using the following equations:

$$A^{**} = \{(maxW_{ij}|j \in J), (minW_{ij}|j \in J')\}; i = 1, 2, \dots, m \tag{10}$$

$$A^* = \{(minW_{ij}|j \in J), (maxW_{ij}|j \in J')\}; i = 1, 2, \dots, m \tag{11}$$

J = 1, 2, 3, n – where J is associated with the most preferable criteria J' = 1, 2, 3, n – where J' is associated with least preferable criteria. The positive ideal solution (A\*\*) is determined based on maximization whereas the unfavourable ideal solution (A\*) is determined based on minimization. According to the present study, the respective most preferable and least preferable ideal solutions are given below,

$$\begin{pmatrix} A^{**} \\ A^* \end{pmatrix} = \begin{pmatrix} 0.0444 & 0.0124 & 0.0576 & 0.0001 & 0.0098 \\ 0.0866 & 0.0349 & 0.0687 & 0.0883 & 0.0393 \end{pmatrix} \tag{12}$$

Step 6: The separation measure is achieved using Eq. (13) and Eq. (14). The same for each alternative from the most preferable ideal solution is given by

$$S_i^{**} = \sqrt{\sum_{j=1}^m (W_{ij} - A_j^{**})^2}, \text{ where } i = 1, 2, \dots, m \tag{13}$$

$$S_i^{**} = \sqrt{(0.0750 - 0.0444)^2 + (0.0200 - 0.0124)^2 + \dots + (0.0162 - 0.0098)^2} = 0.0327 \tag{14}$$

Similarly, the least preferable ideal solution is given by

$$S_i^* = \sqrt{\sum_{j=1}^n (W_{ij} - A_j^*)^2}, \text{ where } i = 1, 2, \dots, m \tag{15}$$

$$S_i^* = \sqrt{(0.0750 - 0.0866)^2 + (0.200 - 0.0349)^2 + \dots + (0.0162 - 0.0393)^2} = 0.0931 \tag{16}$$

Step 7: The relative proximity is evaluated to the ideal solution [Eq. (17)].

$$C_i^* = \frac{S_i^*}{S_i^{**} + S_i^*} \tag{17}$$

$$C_1^* = \frac{0.0327}{0.0931 + 0.0327}$$

$$C_{31}^* = \frac{0.0998}{0.0100 + 0.0998} \tag{18}$$

The uplifted  $C_i^*$  value denotes the best performance of the output response with respect to the input parameters. The separation measure of most preferable, least preferable ideal solutions and the relative closeness values are presented in Table 3.

Step 8: Ranking based on relative closeness value.

A complete ranking of the experimental runs is produced as a result of the computation of the experimental data is 31, 27, 24, 28, 22, 23, 13, 7, 29, 25, 30, 18, 5, 20, 3, 9, 21, 15, 26, 8, 1, 16, 12, 17, 4, 6, 11, 10, 19, and 14. The optimal experimental design is sequenced as 22 > 1 > 18 > 25 > 15 > 26 > 9 > 20 > 16 > 28 > 27 > 29 > 8 > 13 > 17 > 24 > 30 > 12 > 31 > 14 > 21 > 7 > 5 > 4 > 10 > 19 > 2 > 6 > 23 > 11 > 3. It means that the best combination of input parameters is in experimental run 2, and the worst is in experimental run 19. The experimental run 2 has 92.50% relative closeness and run 19 has 34.28%. The superior combination of optimized parameters for the present study is identified in run 2 with an Input current of 180 Amps, Input volt of 17 V, Torch angle of 60 deg, and the welding speed of 125 m/min. Therefore, it is suggested to choose the above parameter setting in order to enhance the quality of weld with respect to mechanical and corrosion resistance properties.

### 3.2 Micro and Macro Study

The microstructure of base alloy 316L consists of an austenitic structure. From the TOPSIS optimization results, the welding conditions of the 2nd experiment with rank 1 (First rank), 5th experiment (middle rank) and the 19th experiment (last rank) were decided then their macro, microstructures and the corrosion rate are discussed here. Fig. 1 (a-c) shows the macrostructures of the cladding specimen for experiments 2, 5, and 19 respectively. The stellite-6 and the base alloy SS316L are shown in Fig. 1a. From the weld bead, the shape and size of the weld bead are different among the experiments as they vary according to the Joining parameters. The molten zone in the base metal was varied. Almost the bead height was varying. From the Fig.s, the 2nd experiment had a low molten zone and bead height compared to the others. The 2nd experiment had a higher current and lower voltage and welding current. The bonding between stellite-6 alloy and SS316L alloy is ensured. No defects were found in the cladding layer.

The cladding surface was analysed by optical microscopy. The optical microstructure of the stellite-6 cladding is shown in Fig. 1 (d-f) for experiments 2, 5, and 19 respectively. All the microstructures are X200 magnification. The microstructure shows the cobalt-based dendrite structure and its variation in size among the experiments. The formation of that structure depended on the welding process and the parameters. This formation may alter the corrosion rate of the specimen. In most cases, a mat-like structure was seen the optical images. The stellite-6 cladding is a good example of having higher corrosion and wear resistance. The uniform distribution of the Co-phase can be seen over the substrate as shown in Fig. 1 (f).

**Table 3 - Separation measure of most preferable, least preferable ideal solutions & relative closeness values**

Number of Run	Separation Measure of Positive Ideal Solution (S <sup>**</sup> )	Separation Measure of Negative Ideal Solution (S <sup>*</sup> )	Relative Closeness (C <sup>*</sup> )	Rank
1	0.032731	0.062851	0.6576	22
2	0.006242	0.077039	0.9250	1
3	0.024503	0.056285	0.6967	18
4	0.036953	0.057797	0.6100	25
5	0.022456	0.061317	0.7319	15
6	0.038078	0.056261	0.5964	26
7	0.017765	0.066785	0.7899	9
8	0.031325	0.063313	0.6690	20

Number of Run	Separation Measure of Positive Ideal Solution (S <sup>**</sup> )	Separation Measure of Negative Ideal Solution (S <sup>*</sup> )	Relative Closeness (C <sup>*</sup> )	Rank
9	0.024472	0.064564	0.7251	16
10	0.04466	0.058595	0.5675	28
11	0.038243	0.056239	0.5952	27
12	0.055369	0.047936	0.4640	29
13	0.015277	0.069991	0.8208	8
14	0.021087	0.061584	0.7449	13
15	0.026003	0.062691	0.7068	17
16	0.03265	0.051823	0.6135	24
17	0.047896	0.038035	0.4426	30
18	0.022001	0.069039	0.7583	12
19	0.063143	0.032934	0.3428	31
20	0.022906	0.066594	0.7441	14
21	0.028086	0.054794	0.6611	21
22	0.01415	0.071659	0.8351	7
23	0.014237	0.072461	0.8358	5
24	0.012662	0.070138	0.8471	4
25	0.019618	0.065909	0.7706	10
26	0.03099	0.06634	0.6816	19
27	0.010332	0.073141	0.8762	2
28	0.013678	0.069492	0.8355	6
29	0.032102	0.057268	0.6408	23
30	0.021504	0.068112	0.7600	11
31	0.010235	0.072088	0.8757	3

The scanning electron microscope (SEM) images of the weld interface region are shown in Fig. 2(a-c) belongs to experiments 2, 5, and 19 respectively. The interface between the SS316L and stellite-6 regions is shown in the Fig.s. The cobalt-based structure was seen on the stellite side. The thickness of the interface was measure in millimetres (mm). The interface thickness of the 2nd experiment, which was having the rank 1 welding conditions according to the TOPSIS optimization, was about 0.05 mm. The other experiments 5, and 19 had the thickness of about 0.092 mm, and 0.076 mm, respectively. From this, it was observed that the higher thickness may reduce the interface property. The 2nd experiment has a uniform and sharp interface compared to the others and stellite alloy is rich in cobalt. The structure formation found in the cladding process was different in the interface region compared to the cladding region and base alloy. The filament-like structure was seen nearby the clad interface is shown in Fig. 2 (e). The 'Co' and 'Cr' based structure is seen in Fig. 2 (f), the thickness of 2-micron size was observed Cr based phase. The structure of the cladding is almost same for the experiments 2, 5, and 19. The hard phases raised the wear and erosion quality of the specimen. The energy-dispersive X-ray spectroscopy (EDS) analysis was done on the specimen produced by experiment number 2 which is having rank 1 through the optimization. Fig. 3 shows the EDS spectrum and the positions where the EDS spectra belong. The rank 1 experiment had a high current of 180 Amps, low voltage of 17 V, low torch angle of about 60 degrees and a low welding speed of 125 m/min. From the results, it had to be understood that the current was playing the major during the experiment. On the specimen, two regions were analysed namely region A and B.

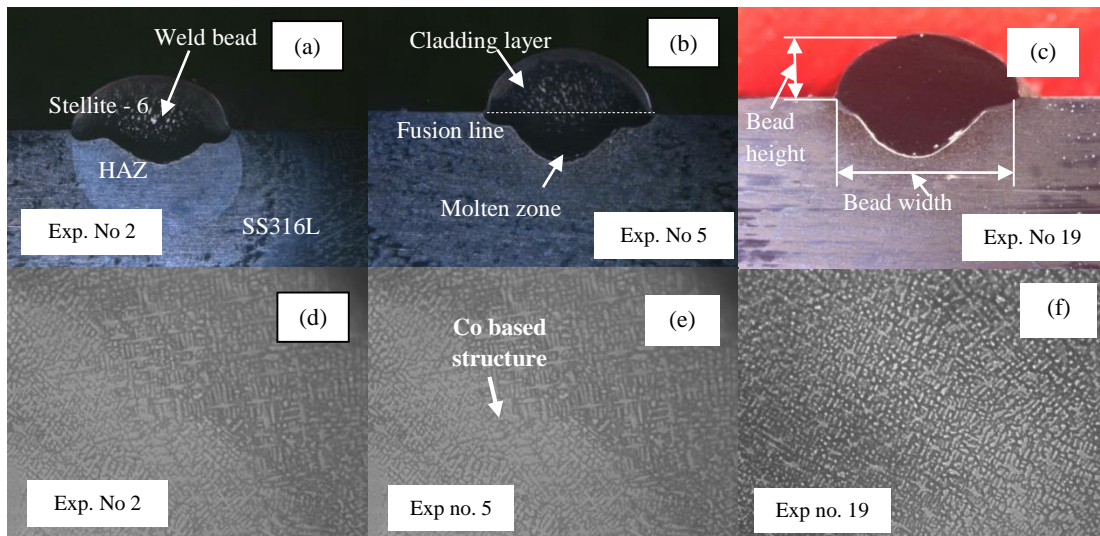


**Fig. 1 (a-e) - Macrostructures of weldment & microstructures of stellite 6 (a & d) exp no 2; (b & e) exp no 5; (c & f) exp no 19**

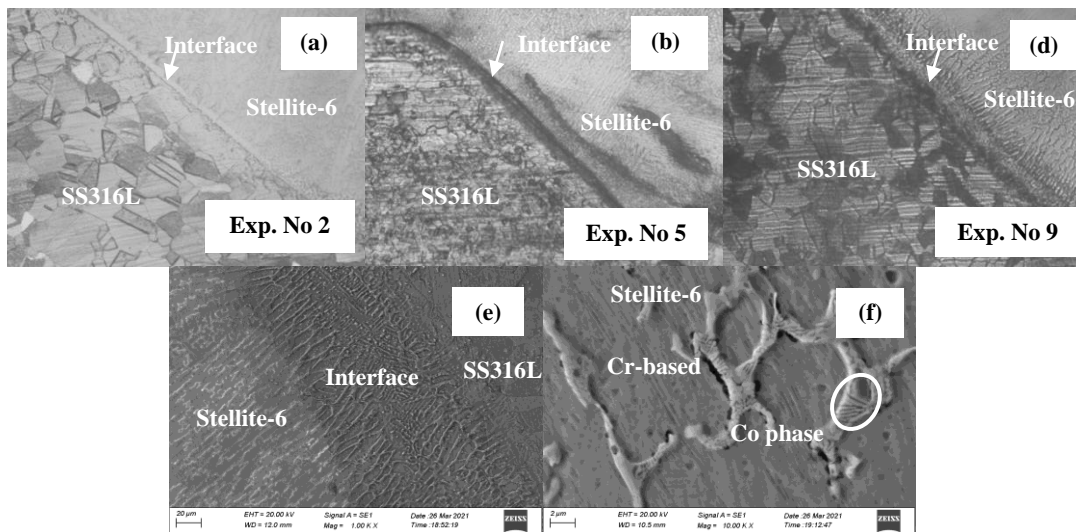


**Fig. 2 (a-e) - The SEM images of weld interface & cladding for the experiments**

Region A is the dendritic-formed structure with ‘Cr’, whereas region B is the Co phase. From the spectra, Co, Fe and a maximum of 38% Cr were found in the region ‘A’. Region ‘B’ consists of 38% Co, 27.8% Fe and 22% Cr.

### 3.3 Corrosion Rate Analysis

The corrosion resistance of the cladding specimen was analysed using the potentiodynamic polarization method with electrochemical impedance-CHI660 A. The analysis graph of the 2nd, 5th, and 19th experiments are shown in Fig. 4 (a-c) respectively. The corrosion rate for the 2nd experiment was 0.004582 mm/yr, for the 5th experiment was 0.01071 mm/yr, and for the 19th experiment was 0.08614 mm/yr. While analysing the experiments the 2nd experiment (first rank) had a higher current of 180 Amps, the 5th experiment (middle rank) had lower welding current but the higher torch of 80° angle, The 19th experiment had the average level of welding conditions like 160 A, low voltage of 15 V, torch angle 70° and the welding speed of 150 m/min. The 2nd experiment yielded a low corrosion rate and having high corrosion resistance. Higher current and lower welding speed provided a low corrosion rate. The Cr and Co phase formation on the clad specimen surface was also influencing the corrosion resistance property. The corrosion rate of the 19th experiment was higher compared to the others. The SEM images of the corroded specimens are shown in Fig. 5. Fig. 5(a) shows the 2nd experiment image of size 30 micron and the corroded area nearby interface was observed. Similarly, the corrode portion on the specimen of experiments 5 & 19 is shown in Fig. 5(b) & 5(c) respectively. The presence of the ‘Cl’ element is seen in the images. The corrosion was not uniform over the surface, instead; corrosion took place in the agglomerated form. The ‘Cr’ and ‘Co’ rich regions showed a low corrosion rate.

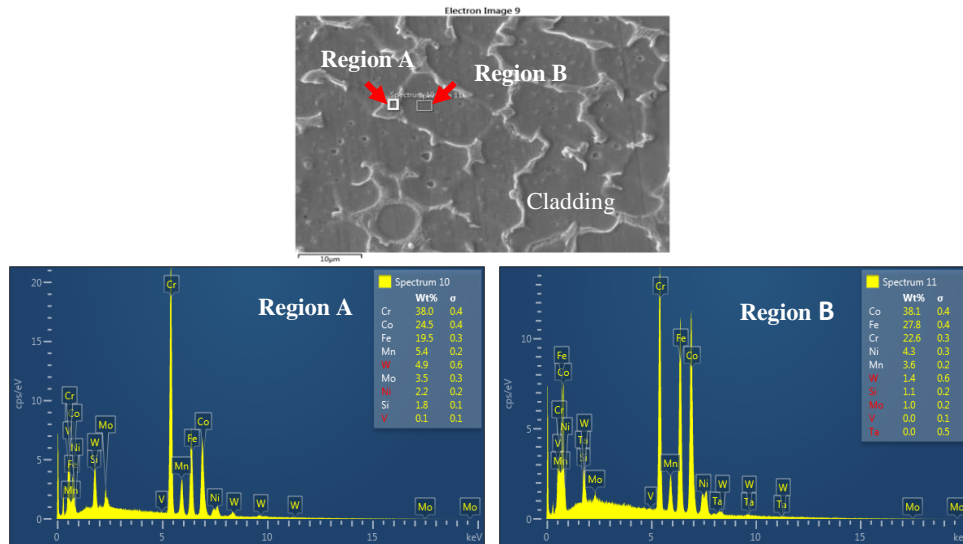


Fig. 3 - SEM image and the EDS spectra on the cladding portion

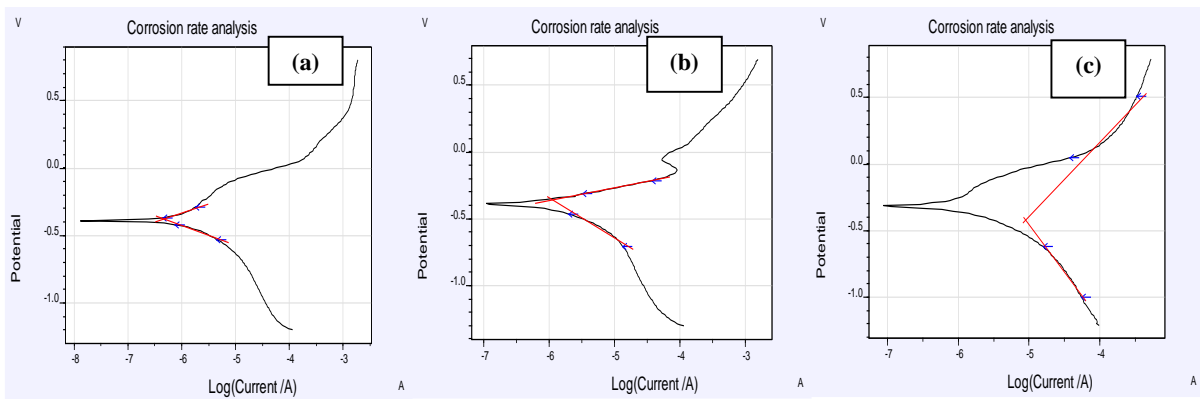


Fig. 4 (a-c) - Corrosion rate analysis (a) exp no 2; (b) exp no 5; (c) exp no 19

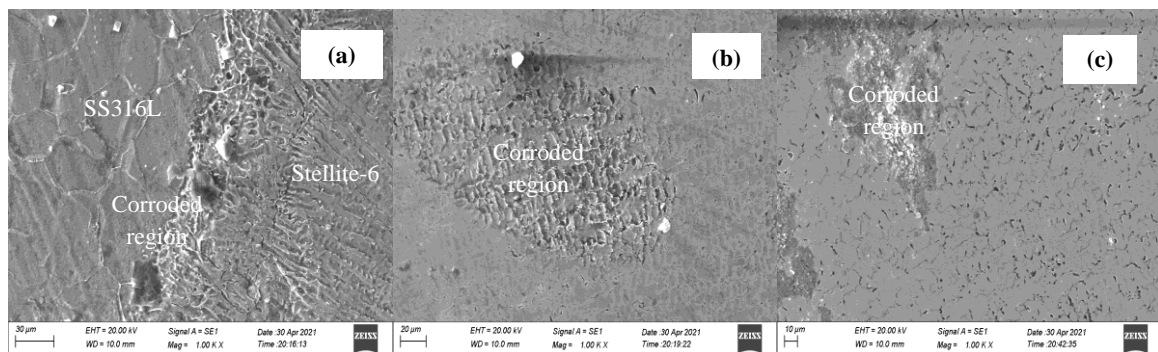


Fig. 5 (a-c) - SEM images of the corroded specimens exp no 2, 5, and 19 respectively

#### 4. Conclusion

The stellite-6 alloy was successfully coated over the metal AISI316L using the CMT cladding method based on CCD and the optimization method TOPSIS was successfully applied. The following results are considered through this investigation.

- a) TOPSIS method helped to rank the CMT cladding experiments and to find the best combination. Experimental run 2 contains the optimal set of input parameters, whereas experimental run 19 contains the unfavourable set.

- b) From the TOPSIS optimization results, the experimental run 2 has 92.50% relative closeness and run 19 has 34.28%. Experiment number 2 was the first rank among the other experiments with higher relative closeness.
- c) The characterisation was done on the best and worst experimental runs' specimens. According to the macro and micro-study, no defects were observed in the cladding regions and interfaces of specimens.
- d) Strong and narrow interfaces were found with a thickness of less than 0.1mm.
- e) In the SEM microstructure, the embedment of the Cr phase in the Co solution is found.
- f) EDS study showed the elements Cr, Co, Fe presence for experiment 2.
- g) The corrosion rate was low for the 2nd experiment compared to the others. The higher current and lower welding speed combination yielded a low corrosion rate.
- h) The 'Cr' and 'Co' rich regions in the specimen showed high corrosion resistance.

**Acknowledgment**

The authors fully acknowledged Research Scholar –Bharath Institute of Higher Education and Research and Research Supervisor –Bharath Institute of Higher Education and Research for supporting this work.

**Appendix A – Model Calculation**

**Step-3** The decision matrix.

$$[D_{31 \times 5}] = \begin{pmatrix} 2.744 & 31.618 & 351 & 0.000781 & 0.079 \\ \cdot & \cdot & \cdot & \cdot & \cdot \\ \cdot & \cdot & \cdot & \cdot & \cdot \\ \cdot & \cdot & \cdot & \cdot & \cdot \\ 1.858 & 30.346 & 336 & 0.004062 & 0.054 \end{pmatrix}$$

$$N_{ij} = \frac{x_{ij}}{\sqrt{\sum_{i=1}^m x_{ij}^2}} \quad j = 1, 2, \dots, n$$

$$N_{1 \times 1} = \frac{2.744}{12.79718} = 0.21422$$

$$N_{1 \times 2} = \frac{31.618}{157.58} = 0.2006$$

$$N_{1 \times 3} = \frac{351}{1930} = 0.18185$$

$$N_{1 \times 4} = \frac{0.00078}{0.1549} = 0.005042$$

$$N_{1 \times 5} = \frac{0.079}{0.4856} = 0.162674$$

**Step 4:** Allocating weights for the entire criterion which are considered for optimization.

$$W_{ij} = N_{ij} \times W_j$$

Where  $N_{ij}$  represents the normalized matrix and  $W_j$  represents the weight criteria. The weights ( $W_j$ ) of each criterion are chosen with the aid of experts. The depth of penetration and hardness is given a weight of 0.35 because they are the most desirable qualities, whereas the other parameters are given a weight of 0.1.

$$W_{1 \times 1} = 0.2144 \times 0.35 = 0.75047$$

$$W_{1 \times 2} = 0.2006 \times 0.1 = 0.02006$$

$$W_{1 \times 3} = 0.1818 \times 0.35 = 0.06365$$

$$W_{1 \times 4} = 0.005042 \times 0.1 = 0.0005$$

$$W_{1 \times 5} = 0.162674 \times 0.1 = 0.01627$$

**Step-5** This step determines the positive ideal ( $A^{**}$ ) and the negative ideal ( $A^*$ ) solutions. These are calculated by using the following equations:

$$A^{**} = \{(max W_{ij} | j \in J), (min W_{ij} | j \in J')\}; i = 1, 2, \dots, m$$

$$A^* = \{(minW_{ij}|j \in J), (maxW_{ij}|j \in J')\}; i = 1, 2, \dots, m$$

A**	0.0444	0.0124	0.0576	0.0001	0.0098
A*	0.0866	0.0349	0.0687	0.0883	0.0393

**Step 6:** The most preferable ideal solution is given by

$$S_i^{**} = \sqrt{\sum_{j=1}^m (W_{ij} - A_j^{**})^2}, \text{ where } i = 1, 2, \dots, m$$

W <sub>ij</sub>	0.07505	0.02006	0.06365	0.0005	0.01627
A**	0.0444	0.0124	0.0576	0.0001	0.0098
A*	0.0866	0.0349	0.0687	0.0883	0.0393

$$S_i^{**} = \text{Sqrt} (0.07505-0.0444)^2+(0.02006-0.0124)^2+(0.06365-0.0576)^2+(0.0005-0.0001)^2 + (0.01627-0.0098)^2 = 0.032731$$

Least preferable ideal solution:

$$S_i^* = \sqrt{\sum_{j=1}^n (W_{ij} - A_j^*)^2}, \text{ where } i = 1, 2, \dots, m$$

$$S_i^* = \text{Sqrt}(0.07505-0.0866)^2+(0.02006-0.0349)^2+(0.06365-0.0687)^2+(0.0005-0.0883)^2+(0.01627-0.0393)^2 = 0.062851$$

**Step 7:** Relative closeness value.

$$C_i^* = \frac{S_i^{**}}{S_i^{**} + S_i^*}$$

$$C_1^* = \frac{0.032731}{0.062851 + 0.032731} = 0.6576$$

## References

- [1] Guojian Xu, Muneharu Kutsuna, Zhongjie Liu, Katsusige Yamada (2006). Comparison between diode laser and TIG cladding of Co-based alloys on the SUS403 stainless steel. *Surface and Coatings Technology*, 201 (3–4), 1138–1144. DOI: 10.1016/j.surfcoat.2006.01.040
- [2] C.R.C. Lima, M.J.X. Belém, H.D.C. Fals, C.A. Della Rovere (2020). Wear and corrosion performance of Stellite 6 coatings applied by HVOF spraying and GTAW hotwire cladding. *Journal of Materials Processing Technology*. 284, 116734. DOI: 10.1016/j.jmatprotec.2020.116734
- [3] Evangeline, A., Sathiya, P. & Arivazhagan, B. (2020). Laves Phase Formation and Segregation of Nb in Ni–Cr–Mo Super alloy over 316L by Hot Wire (HW) TIG Cladding Process. *Arab J Sci Eng*. 45, 9685–9698. <https://doi.org/10.1007/s13369-020-04873-0>
- [4] Mohammed, S., Zhang, Z. & Kovacevic, R. (2020). Optimization of processing parameters in fiber laser cladding. *Int J Adv Manuf Technol*. 111, 2553–2568. <https://doi.org/10.1007/s00170-020-06214-9>
- [5] G.R. Mirshekari, S. Daei, S. Fatoureh Bonabi, M.R. Tavakoli, A. Shafyei, M. Safaei (2017). Effect of interlayers on the microstructure and wear resistance of Stellite 6 coatings deposited on AISI 420 stainless steel by GTAW technique. *Surfaces and Interfaces*. 9, 79–92. DOI: 10.1016/j.surf.2017.08.005
- [6] Yin, X., He, G., Meng, W. et al. (2020). Comparison Study of Low-Heat-Input Wire Arc-Fabricated Nickel-Based Alloy by Cold Metal Transfer and Plasma Arc. *J. of Materi Eng and Perform*. 29, 4222–4232. <https://doi.org/10.1007/s11665-020-04942-3>
- [7] Dutra, J.C., Silva, R.H.G.e., Marques, C. et al. (2016). A new approach for MIG/MAG cladding with Inconel 625. *Weld World*. 60, 1201–1209. <https://doi.org/10.1007/s40194-016-0371-3>

- [8] Zinke, M., Burger, S., Arnhold, J. et al. (2021). Effect of different variants of filler metal S Ni 6625 on properties and microstructure by additive layer manufactured using CMT process. *Weld World*. 65, 1553–1569. <https://doi.org/10.1007/s40194-021-01105-3>
- [9] P. Ganesh, A. Moitra, Pragya Tiwari, S. Sathyanarayanan, Harish Kumar, S.K. Rai, Rakesh Kaul, C.P. Paul, R.C. Prasad, L.M. Kukreja (2010). Fracture behavior of laser-clad joint of Stellite 21 on AISI 316L stainless steel. *Materials Science and Engineering: A*. 527 (16–17), 3748-3756. DOI: [10.1016/j.msea.2010.03.017](https://doi.org/10.1016/j.msea.2010.03.017)
- [10] G.P. Rajeev, M. Kamaraj, Srinivasa R. Bakshi (2017). Hardfacing of AISI H13 tool steel with Stellite 21 alloy using cold metal transfer welding process. *Surface & Coatings Technology*. DOI: [10.1016/j.surfcoat.2017.07.050](https://doi.org/10.1016/j.surfcoat.2017.07.050)
- [11] Anish Nair, V. Ramji, R. Durai Raj, R. Veeramani (2021). Laser cladding of Stellite 6 on EN8 steel – A fuzzy modelling approach. *Materials Today: Proceedings*. 39 (1), 348-353. DOI: [10.1016/j.matpr.2020.07.431](https://doi.org/10.1016/j.matpr.2020.07.431)
- [12] Rajeev, G.P., Kamaraj, M. & Bakshi, S.R. (2014). Al-Si-Mn Alloy Coating on Aluminum Substrate Using Cold Metal Transfer (CMT) Welding Technique. *JOM*. 66, 1061–1067. <https://doi.org/10.1007/s11837-014-0970-7>
- [13] F. Madadi, F. Ashrafzadeh, M. Shamanian (2012). Optimization of pulsed TIG cladding process of stellite alloy on carbon steel using RSM. *Journal of Alloys and Compounds*. 510 (1), 71-77. DOI: [10.1016/j.jallcom.2011.08.073](https://doi.org/10.1016/j.jallcom.2011.08.073)
- [14] Muhammad Akram, Arooj Adeel, and José Carlos R (2019). Alcantud Multi-Criteria Group Decision-Making Using an m-Polar Hesitant Fuzzy TOPSIS Approach Symmetry. *MDPI*. 11, 795. DOI: [10.3390/sym11060795](https://doi.org/10.3390/sym11060795)
- [15] Berna (Kiran) (2012). Bulgurcu Application of TOPSIS Technique for Financial Performance Evaluation of Technology Firms in Istanbul Stock Exchange Market. *Procedia - Social and Behavioral Sciences*. 62, 1033 – 1040. DOI: [10.1016/j.sbspro.2012.09.176](https://doi.org/10.1016/j.sbspro.2012.09.176)
- [16] Renato A. Krohling, André G.C. Pacheco (2015). A-TOPSIS – An Approach Based on TOPSIS for Ranking Evolutionary Algorithms. *Procedia Computer Science*, 55, 308-317. DOI: [10.1016/j.procs.2015.07.054](https://doi.org/10.1016/j.procs.2015.07.054)
- [17] Robbi Rahim et al (2018). TOPSIS Method Application for Decision Support System in Internal Control for Selecting Best Employees. *IOP Conf. Series: Journal of Physics: Conference Series*. 1028, 012052. DOI: [10.1088/1742-6596/1028/1/012052](https://doi.org/10.1088/1742-6596/1028/1/012052)
- [18] Xing Zhongyou (2012). Study on the Application of TOPSIS Method to the Introduction of Foreign Players in CBA Games. *Physics Procedia*. Volume 33, p 2034-2039. DOI: [10.1016/j.phpro.2012.05.320](https://doi.org/10.1016/j.phpro.2012.05.320)
- [19] Liguofei, Yong Hu, Fuyuan Xiao, Luyuan Chen, and Yong Deng (2016). A Modified TOPSIS Method Based on D Numbers and Its Applications in Human Resources Selection. *Mathematical Problems in Engineering*. 6145196, 14, DOI: [10.1155/2016/6145196](https://doi.org/10.1155/2016/6145196)
- [20] Dariusz Kacprzak (2020). An extended TOPSIS method based on ordered fuzzy numbers for group decision making. *Artif Intell Rev*. 53, 2099–2129, DOI: [10.1007/s10462-019-09728-1](https://doi.org/10.1007/s10462-019-09728-1)
- [21] Peng Wang, Yang Li, Yong-Hu Wang, Zhou-Quan Zhu (2015). A New Method Based on TOPSIS and Response Surface Method for MCDM Problems with Interval Numbers. *Mathematical Problems in Engineering*. 938535, 11. DOI: [10.1155/2015/938535](https://doi.org/10.1155/2015/938535)
- [22] Marzban, J., Ghaseminejad, P., Ahmadzadeh, M.H. et al. (2015). Experimental investigation and statistical optimization of laser surface cladding parameters. *Int J Adv Manuf Technol*. 76, 1163–1172. <https://doi.org/10.1007/s00170-014-6338-x>.
- [23] S. Ramesh, R. Viswanathan, S. Ambika, Measurement and optimization of surface roughness and toolwear via grey relational analysis, TOPSIS and RSA techniques, *Measurement* 78, (2016), 63-72. <https://doi.org/10.1016/j.measurement.2015.09.036>
- [24] Ramesh, S., Boppana, S.B., Manjunath, A. K. Parthiban Corrosion Behavior Studies and Parameter Optimization of Dissimilar Alloys Joined by Electron Beam Welding. *J Bio Tribo Corros* 6, 73 (2020), <https://doi.org/10.1007/s40735-020-00372-9>.
- [25] H. So, C.T. Chen, Y.A. Chen (1996). Wear behaviors of laser-clad stellite alloy 6. *Wear*. 192, 78-84.
- [26] Raghuvir Singh, Damodar Kumar, S.K. Mishra, S.K. Tiwari (2014). Laser cladding of Stellite 6 on stainless steel to enhance solid particle erosion and cavitation resistance. *Surface and Coatings Technology*. 251, 87-97. DOI: [10.1016/j.surfcoat.2014.04.008](https://doi.org/10.1016/j.surfcoat.2014.04.008)
- [27] Senthil, M.S., Noorul, H.A., Sathiya, P (2020). Eco-friendly frictional joining of AA6063 and AISI304L dissimilar metals and characterization of bimetal joints. *Journal of New Materials for Electrochemical Systems*. 23 (No. 2), 101-111. DOI: [10.14447/jnmes.v23i2.a07](https://doi.org/10.14447/jnmes.v23i2.a07)